Electrochimica Acta 556 (2026) 148424

Contents lists available at ScienceDirect

Electrochimica Acta

journal homepage: www.journals.elsevier.com/electrochimica-acta

Efficient and facile electrochemical synthesis of sodium perborate using boron-doped diamond anode

Ziqi Teng [a], Finn Moeller [a], Siegfried R. Waldvogel [a,b,*]

[a] Max-Planck-Institute for Chemical Energy Conversion, Department of Electrosynthesis, Stiftstraße 34-36, 45470 Mülheim an der Ruhr Germany
[b] Karlsruhe Institute of Technology, Institute of Biological and Chemical Systems – Functional Molecular Systems (IBCS–FMS), Kaiserstraße 12, 76131 Karlsruhe Germany

ARTICLE INFO

Keywords:
Electrosynthesis
Platform oxidizer
Perborate monohydrate
Peroxodicarbonate
Diamond electrodes

ABSTRACT

Electrochemical oxidation offers a sustainable alternative to conventional oxidant production. Yet, the electrosynthesis of sodium perborate (SPB) has remained difficult due to its narrow stability window in aqueous solution and competition of oxygen evolution reaction under high potential. Although boron-doped diamond (BDD) electrodes are well known for enabling high-potential anodic reactions, their applicability to perborate synthesis has previously been questioned. Here, we demonstrate a robust, reproducible, and practical one-step electrochemical route to sodium perborate monohydrate (SPB-1) that directly yields a stable crystalline product using a BDD anode in concentrated carbonate/bicarbonate electrolytes. Systematic variation of operating parameters reveals that low temperature (3.5 °C), moderate-to-high current density (0.825–0.875 A cm^{-2}), controlled amount of the applied charge (24–26 *F*), and sufficient post-electrolysis mixing (>20 min) are essential for efficient perborate formation. Under optimized conditions, the process achieves an isolated yield of 79 ± 3%, an active oxygen content of 14.0 ± 0.6%, and a current efficiency of 26 ± 1% across five independent runs, demonstrating excellent reproducibility and product quality comparable to commercial SPB-1. Cyclic voltammetry and galvanostatic anode potential measurements reveal that carbonate oxidation on BDD occurs at highly positive potentials overlapping with the oxygen evolution region, rationalizing the narrow optimal current density window and the superior performance of BDD relative to platinum anodes. FTIR analysis confirms the formation of SPB-1, with all characteristic vibrational features matching those of authentic material. Overall, this work establishes a reliable electrochemical strategy for SPB-1 synthesis, supported by mechanistic insight and quantitative benchmarking, and highlights the potential of BDD-based electrolysis for sustainable and scalable oxidant production.

1. Introduction

Sodium perborate (SPB) is a cyclic disubstituted peroxide widely used as a stable and solid alternative to hydrogen peroxide due to its low cost, long shelf life, safety, and ease of handling [1–3]. It finds broad industrial applications in bleaching, household and medical cleaning agents, toothpaste, and cosmetics [3–7]. More recently, SPB has attracted attention for emerging uses in hydraulic fracturing, fuel cells, batteries, and aquaculture [7]. Since the 1980s, it has also become increasingly important in organic synthesis—typically in acetic or other carboxylic acids [8]—where it enables diverse oxidation reactions, including sulfide oxidation [9], N-hydroxylation of azoles [10], conversion of oximes to carbonyl compounds [11], and oxidation of organoboranes [2].

Industrial SPB production is well established. In the conventional route [12–14], borax ($Na_2B_4O_7{\cdot}10H_2O$) is converted in alkaline media into soluble metaborate species, which are then oxidized with hydrogen peroxide or sodium peroxide to produce SPB tetrahydrate. However, this process is energy-intensive because hydrogen peroxide is itself produced via the anthraquinone process [15]. The synthesis additionally requires strict temperature control (<15 °C) to maintain product quality during the highly exothermic reaction [16]. Handling concentrated oxidizers and managing the resulting wastewater streams introduce further safety and environmental concerns [13]. These drawbacks highlight the need

* Corresponding author.
E-mail address: siegfried.waldvogel@cec.mpg.de (S.R. Waldvogel).
URL: http://www.cec.mpg.de/de/forschung/elektrosynthese (S.R. Waldvogel).

https://doi.org/10.1016/j.electacta.2026.148424
Received 20 December 2025; Received in revised form 27 January 2026; Accepted 8 February 2026
Available online 9 February 2026

for a greener, more direct, and sustainable pathway for SPB production.

Electrochemical synthesis experiences currently a renaissance and considered because of valorization by intermittent electricity from renewable resources a future technology [17]. The electrosynthetic approach offers such a possibility and has been explored for more than a century. In 1916, Arndt [18] demonstrated electrochemical SPB formation from borax and sodium carbonate. Subsequent studies by Liebknecht [19], Regner [12], Mollard [20], and Mohan Rao and Rachavendran [21–22] investigated electrolyte composition, pretreatments, and operational parameters such as temperature and current density. However, these works consistently reported challenges in obtaining stable perborate and relied predominantly on platinum anodes [3,12,20–22].

Although platinum is widely used due to its conductivity, catalytic activity, and apparent stability [23–24], these same properties can be disadvantageous in oxidative systems. Its high catalytic activity promotes oxygen evolution and non-selective oxidation reactions [25–26], lowering selectivity and current efficiency. Moreover, platinum is not entirely stable: at high anodic potentials it undergoes surface oxidation and gradual dissolution in both, acidic and alkaline media [27–30]. Trace metal impurities such as Mn, Fe, or Cu—commonly present in commercial borax—can further deposit on Pt surfaces and inhibit activity [31]. Regner [12] observed significant losses in current efficiency under such conditions, and Mollard [20] showed that stabilizers such as magnesium nitrate and urea can partially mitigate Pt consumption. Although commercial borax nowadays is typically of high purity (>99%) and contains only trace iron impurities (≤0.0005 wt%), which reduces impurity-driven degradation. Despite the high purity of commercial borax, platinum anodes are not well suited for sustained and scalable perborate electrosynthesis due to their scarcity and supply risk [32], limited durability under high anodic polarization [33], and strong competition from OER.

Semi-conducting diamond has emerged as a highly promising electrode material due to its exceptional hardness, chemical inertness, and tunable conductivity [34–37]. Advances in chemical vapor deposition (CVD) now allow the fabrication of boron-doped diamond (BDD) thin films, where heavy boron incorporation imparts semi-metallic behavior [36–37]. By contrast to Pt, BDD electrodes are composed of abundant elements (B and C) and can be produced at scale using CVD techniques, offering improved availability and scalability for industrial applications [34–35]. In addition, BDD electrodes offer several advantages over conventional materials, including an ultra-wide potential window [38–41], outstanding chemical stability even in strongly acidic environments [36–38,42–44], very low background currents [39,45], and long operational lifetimes owing to minimal adsorption and excellent resistance to surface deactivation [39,46]. Oxidation processes at BDD proceed primarily via weakly adsorbed hydroxyl radicals, which provide strong yet non-destructive oxidizing power [44,47–51]. This unique reactivity enables highly selective oxidation without significant electrode degradation, making BDD particularly effective in advanced oxidation processes and electro-peroxide synthesis [47–55].

Owing to these properties, BDD anodes have attracted increasing attention for high-potential electrochemical oxidation and the generation of inorganic peroxide and peroxy-species. Recent authoritative reviews have highlighted BDD as a benchmark platform for such transformations, particularly in the electrosynthesis of peroxodicarbonate and related oxidants with emerging green industrial relevance [56]. Mechanistic studies have demonstrated that •OH radicals play a central role in water oxidation on BDD, enabling the formation of CO_2, H_2O_2, and O_2 depending on electrolyte composition and operating conditions [57]. BDD has further been shown to produce hydrogen peroxide via both two-electron water oxidation and oxygen reduction pathways [58]. Beyond H_2O_2 formation [57–59], BDD is especially effective for generating peroxodicarbonate ($C_2O_6^{2-}$) in carbonate electrolytes, a key intermediate directly relevant to sodium perborate formation. Following the initial report by Nishiki and Saha, who achieved current efficiencies up to 81% [60], subsequent studies revealed strong influences of temperature and current density on peroxodicarbonate stability [61–62]. More recently, Waldvogel, Gooßen, and co-workers demonstrated highly efficient peroxodicarbonate generation at elevated current densities using temperature-controlled BDD-based flow systems, reaching concentrations above 0.9 M [63]. Importantly, electrogenerated peroxodicarbonate has been successfully applied as an on-demand oxidant for a wide range of sustainable organic transformations, underscoring the broader relevance of BDD-enabled inorganic peroxide chemistry [61–70]. From an industrial perspective, this chemistry is particularly attractive, as the carbonate released after oxidation can be directly recycled as a make-up chemical in Kraft pulping processes [55].

Because both hydrogen peroxide and peroxodicarbonate serve as intermediates in sodium perborate formation, these findings strongly suggest that BDD electrodes could enable a stable and efficient anodic platform for direct electrochemical SPB synthesis. Although González Pérez et al. [3] previously claimed that BDD was unsuitable for perborate production, our study demonstrates—for the first time—a practical, one-step electrochemical synthesis of sodium perborate using BDD anodes under mild conditions, establishing a sustainable route that does not rely on externally supplied oxidants. This approach inherently avoids the production, concentration, transport, and storage of hydrogen peroxide, thereby reducing process complexity and associated safety and energy penalties.

From an energy and sustainability perspective, the anodic formation of peroxy-compounds represents a value-added alternative to the OER. Whereas OER proceeds at a thermodynamic potential of 1.23 V vs RHE and typically requires substantial overpotential to generate low-value O_2, replacing OER with productive peroxy-compound formation converts electrical energy directly into a chemically stored oxidizing equivalent [71–72]. In addition, pairing perborate synthesis at the anode with hydrogen evolution at the cathode enables the simultaneous generation of a valuable oxidant and green H_2, an energy-dense fuel or chemical feedstock. This dual-product configuration improves overall energy utilization and strengthens the case for electrochemical SPB production as a sustainable process that integrates oxidant synthesis with renewable hydrogen generation [73–76].

2. Experimental methodology

Electrolysis was conducted in a 100 mL undivided cylindrical glass cell equipped with a cooling jacket connected to a thermostat (Julabo 200F) for precise temperature control (Fig. 1) [77]. A commercial boron-doped diamond (BDD) electrode (DIACHEM®, Condias GmbH; 10

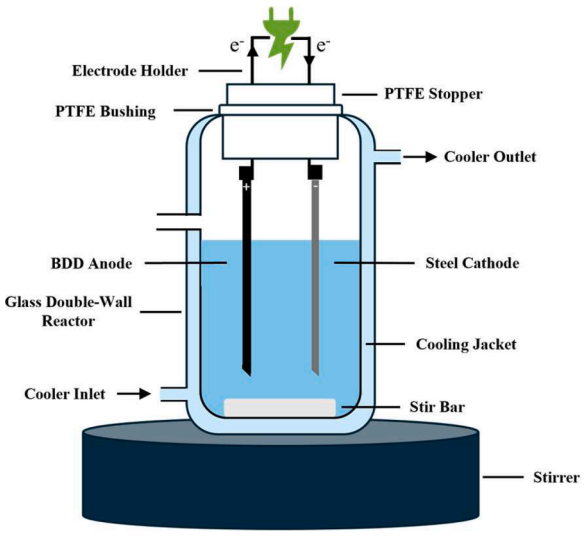

Fig. 1. Schematic picture for the electrochemical cell generating perborate.

× 70 × 3 mm; active area 5.2 cm^2) consisting of a boron-doped polycrystalline diamond film on a silicon substrate was used as the anode. The film is predominantly sp^3-hybridized, with a minor sp^2 contribution typical of conductive BDD electrodes. A stainless-steel plate of identical size was used as the cathode. The electrolyte consisted of 100 mL of an aqueous solution containing 130 g L^{-1} Na_2CO_3 and 30 g L^{-1} $NaHCO_3$. Borax (40 g L^{-1}, Thermo Scientific or Sigma-Aldrich, with the purity over 99% and the content of Pb $\leq$ 0.001% and Fe$\leq$ 0.005%) was directly added to the cell prior to electrolysis without pretreatment. All experiments were performed under galvanostatic conditions.

Cyclic voltammetry shows no discernible cathodic reduction peak attributable to SPB-1 prior to the onset of the HER (Fig. S8), indicating that direct electrochemical reduction of perborate is kinetically negligible compared to HER under the applied conditions. In addition, stable active oxygen contents and reproducible perborate yields were consistently obtained during galvanostatic electrolysis, further supporting that cathodic degradation does not significantly affect the product. On this basis, the use of an undivided cell configuration is most efficient for the presented study.

After electrolysis, the crude solid product was collected by filtration through a glass frit, transferred to Petri dishes, and dried overnight at 55 °C. During drying, volatile or unstable peroxo species such as H_2O_2 and peroxodicarbonate decompose or evaporate, leaving SPB as the sole stable peroxo species in the isolated solid.

To gain further electrochemical insight into the observed trends, the anode potential was monitored during galvanostatic electrolysis against an Ag/AgCl (3 M KCl) reference electrode while varying current density, temperature, and electrolyte concentration (Table S2-S5). These experiments were conducted in a reduced electrolyte volume (40 mL) compared to the 100 mL synthesis cell, due to the current limitation of the potentiostat used (PARSTAT 4000A, AMETEK). Consequently, the absolute anode potentials differ from those in the synthesis configuration (Table S5); however, relative trends with operating parameters are robust and provide mechanistic insight. All potentials reported below are therefore discussed qualitatively in terms of trends rather than absolute threshold values.

The active oxygen content (AOC) of the product was quantified using the established iodometric titration method (Supplementary) [63,78]. The theoretical AOC of sodium perborate monohydrate (SPB-1) is 16%, and commercial samples typically show values between 14–16% [7,79]. The standard SPB-1 sample used in this study (Sigma-Aldrich) exhibited an AOC of 14.0% by iodometric titration.

Fourier-transform infrared (FTIR) spectroscopy (Bruker Alpha) was used to qualitatively characterize the solid product and compare it with commercial SPB-1. Additional analyses using ^{11}B NMR spectroscopy were evaluated for potential quantitative application; however, due to signal instability and poor reproducibility, this method was not pursued for quantification [80–83].

3. Results and conclusion

3.1. SPB synthesis on BDD electrodes and key operational parameters

To identify optimal conditions for electrochemical sodium perborate synthesis, the effects of temperature, current density, charge, and mixing were systematically screened (Fig. 2). For parameter screening, different amounts of applied charge were intentionally employed depending on the variable investigated. Current density was screened at a lower applied charge of 8 *F*, corresponding to the theoretical charge required for conversion of one mole of borax to perborate, in order to minimize the possible impact from secondary processes (e.g., oxygen evolution and peroxide decomposition) and enhance sensitivity to differences in faradaic efficiency. For investigation of post-electrolysis stirring speed, a moderately higher charge of 14 F was applied to increase the amount of perborate formed and thereby improve the resolution of yield differences. Following identification of suitable operating windows, higher applied amount of charges (24–26 *F*) were subsequently used to maximize isolated yield and define the final optimized conditions.

Temperature had the strongest influence on product formation (Fig. 2a). Cooling the electrolyte from an internal temperature of 25 °C to 2.5 °C markedly improved both yield and AOC, consistent with

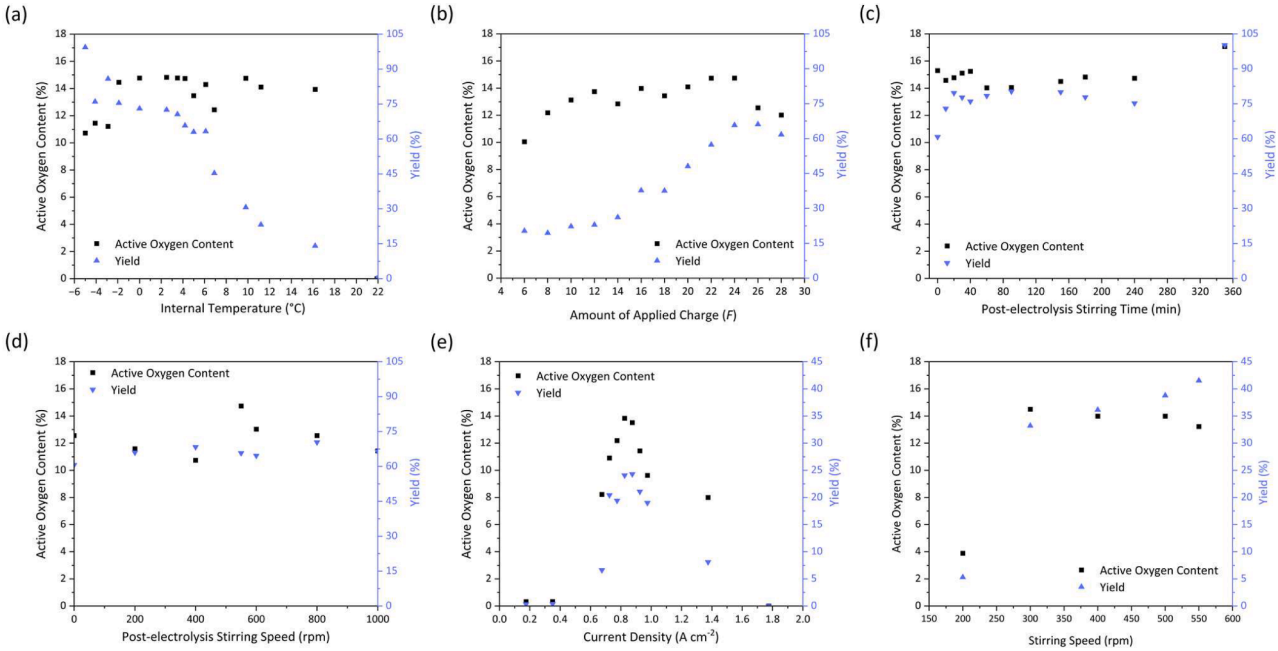

Fig. 2. Optimization of electrolysis parameters for sodium perborate synthesis. Electrolyses were conducted in an undivided batch cell equipped with a BDD anode and a stainless-steel cathode, using an electrolyte of 40 g L^{-1} $Na_2B_4O_7{\cdot}10H_2O$, 130 g L^{-1} Na_2CO_3, and 30 g L^{-1} $NaHCO_3$ in deionized water, performed standardly at 0.875 A cm^{-2}, 550 rpm, 24 *F*, inert temperature of 4.2 °C, followed by 30 min post-electrolysis stirring at 550 rpm. (a) Temperature dependence. A comparison of set vs. internal temperatures is provided in Table S1. (b) Effect of the amount of applied charge (c) Effect of post-electrolysis stirring time. (d) Effect of post-electrolysis stirring speed. (e) Current density dependence, performed at 8 *F*. (f) Effect of post-electrolysis stirring speed, conducted at 14 *F*.

improved stability of SPB as well es stability of peroxodicarbonate and suppression of its decomposition into hydrogen peroxide. No product was obtained at room temperature; precipitation occurred only below 16 °C, with the highest yields at 2.5 °C. Further cooling provided minimal additional benefit, whereas temperatures below −1.9 °C caused carbonate crystallization due to supersaturation, as confirmed by IR analysis (Section 3.2).

Current density also played a crucial role (Fig. 2e). The highest yields and AOC values were obtained at 0.825–0.875 A cm^{-2}. At lower current densities (<0.6 A cm^{-2}), no solid product formed, suggesting insufficient anodic oxidation of carbonate to peroxodicarbonate. Excessively high current densities, however, favored oxygen evolution and peroxide degradation, decreasing efficiency.

These trends are consistent with the corresponding galvanostatic anode potential measurements. The sharp increase in anode potential at high current density indicates that the anode is driven into an increasingly extreme oxidation regime. As shown by cyclic voltammetry (Fig. 6), the onset of anodic oxidation in carbonate/bicarbonate electrolytes occurs at high positive potentials that overlap with the OER region. This indicates that a high anodic potential is required to generate the relevant carbonate-derived peroxy-intermediates; however, once the potential becomes excessively high, competition from OER increasingly dominates. Consequently, the optimal current density represents a compromise: sufficiently high anodic driving force to enable peroxy-species formation, but not so high that nonselective OER and peroxide degradation prevail.

Temperature-dependent galvanostatic measurements show that, at a fixed current density of 0.875 A cm^{-2}, decreasing the electrolyte temperature leads to a systematic increase in the apparent anode potential (from ~4.9 V vs RHE at room temperature to ~7.1 V at −1.9 °C; Table S3). This trend is expected under galvanostatic control due to increased solution resistance and slower interfacial kinetics at lower temperature. Importantly, the highest perborate yields were obtained not at the lowest temperature but at an intermediate internal temperature of ~3.5 °C, indicating that improved performance cannot be ascribed solely to higher anodic potentials. Instead, the enhanced yield at reduced temperature is more consistently attributed to increased chemical stability of carbonate-derived peroxy intermediates and sodium perborate, whereas excessively low temperatures impose practical limitations such as salt crystallization and mass-transport constraints.

The effect of the total amount of applied charge followed a similar trend (Fig. 2b). Yields increased with charge up to 24–26 *F* and declined thereafter. At 28 *F*, diminished perborate-specific IR signals indicated that additional charge neither improved yield nor product quality and may promote decomposition.

Efficient mixing was essential for maintaining homogeneity and ensuring rapid interaction between free borate and the in situ generated H_2O_2 (Fig. 2e), implementing a flow-based setup could further enhance mass transport and mixing efficiency, which may be beneficial [84].

High stirring speeds during electrolysis improved both product yield and AOC. Post-electrolysis mixing, by contrast, required only moderate agitation; 0 rpm still resulted in >60% yield, while 200–600 rpm stabilized yields near 65–70% (Fig. 2d).

Post-electrolysis stirring time also significantly influenced conversion (Fig. 2c). Short stirring times (≤20 min) resulted in incomplete conversion, with substantially lower AOC and yield, whereas characteristic SPB spectral features and AOC values stabilized after approximately 20 min, reaching a consistent range of 12–14%. Prolonged stirring (up to 6 h) led to an apparent increase in AOC and nearly quantitative yields; however, this effect is attributed to carbonate precipitation at low temperature and inhomogeneous sampling rather than true enhancement of perborate formation, as supported by IR analysis (Fig. 5).

Visually, the electrolyte became progressively more opaquer during the first ~20 min following electrolysis, with gradual thickening of the suspended solid phase. This observation is consistent with the second, non-electrochemical step discussed in the mechanistic section, in which residual H_2O_2 generated during electrolysis requires sufficient time to interact with free borate species remaining in solution to form stable sodium perborate.

Unlike previous reports in which silicate stabilizers enhanced performance [12,20,22], the addition of stabilizing agents in this study provided only marginal or negative effects (Table S6).

Overall, the key parameters for high yield and complete conversion are low electrolyte temperatures (preferably <4 °C), strong stirring during electrolysis, current densities of 0.825–0.875 A cm^{-2}, and ≥20 min of post-electrolysis stirring.

Under optimized conditions (0.875 A cm^{-2}, 24 F, 550 rpm, followed by 30 min of post-electrolysis stirring), the synthesis showed excellent reproducibility (Fig. 3). Across five independent runs at an internal temperature of 3.5 °C, the system achieved an average AOC of 14.0 ± 0.6%, slightly exceeding the commercial reference, a yield of 79 ± 3%, and a current efficiency of 26.4 ± 1.0%. The electrolysis operated at an average cell voltage of approximately 12.4 V (Fig. S9) under optimized condition, This translates to a specific energy consumption of 2.46 kWh mol^{-1}, or 24.6 kWh kg^{-1} of SPB-1. The narrow standard deviations confirm the robustness and operational stability of the process and highlight its suitability for practical and scalable oxidant production.

For comparison, electrolysis performed under identical conditions using a platinum anode with the same geometric active area resulted in a product with an oxygen content (AOC) of 11.2% and a yield of 59.0%. Notably, the apparent anode potential measured against Ag/AgCl was substantially lower for Pt (≈4.3 V vs RHE) than for BDD (≈6.4 V vs RHE). This lower anodic potential places Pt predominantly in the oxygen evolution regime, where OER is kinetically favored due to the intrinsically low OER overpotential of Pt (≈1.6 V vs RHE in 0.1 M $HClO_4$ [85]). Consequently, the anodic current on Pt is largely consumed by water oxidation rather than by the high-potential carbonate oxidation pathways required to generate carbonate-derived peroxy-intermediates. These results underscore the critical role of the wide anodic potential window of BDD in enabling selective peroxy-species generation and explain the worse performance of Pt under otherwise identical conditions.

3.2. *Characterization of the product*

FTIR spectroscopy was used to qualitatively verify product identity by comparing spectra of synthesized solids with commercial SPB-1 and

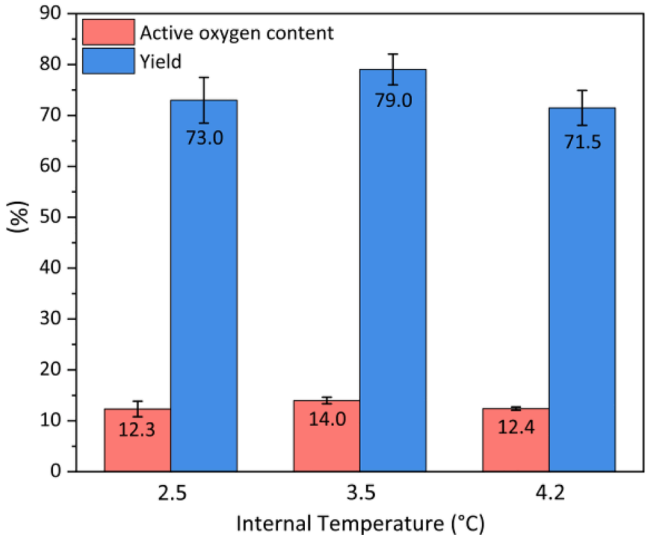

Fig. 3. Reproducibility of the electrosynthesis of sodium perborate. The electrolysis was repeated five times under identical conditions, and each isolated product was quantified by triplicate iodometric titration.

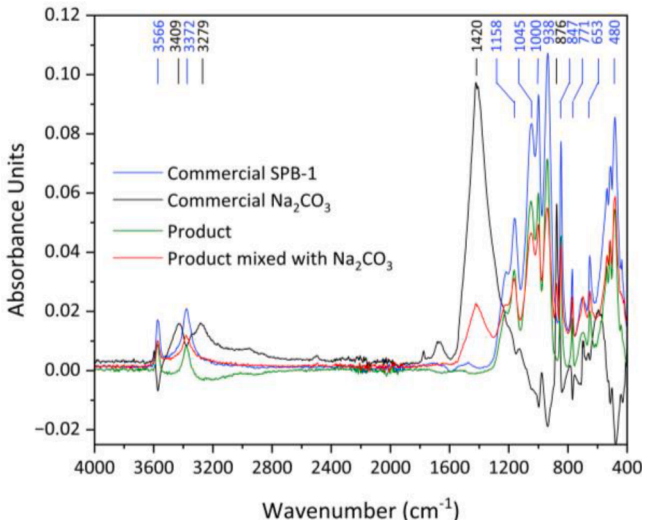

Fig. 4. FTIR comparison of synthesized sodium perborate with reference materials. Spectra are shown for commercial SPB-1, sodium carbonate, the electrochemically synthesized product obtained under optimized conditions, and a mixture of synthesized product with commercial sodium carbonate.

relevant reference materials. Fig. 4 displays spectra of SPB-1, sodium carbonate, the product after isolation under optimized conditions, and a mixture of synthesized product with sodium carbonate.

Commercial SPB-1 displays characteristic fingerprint-region bands (1200–400 cm^{-1}) associated with B–O stretching/bending of BO_3/BO_4 units and B–O–H vibrations, along with O–H stretching at 3566 and 3372 cm^{-1} [86–87]. Sodium carbonate features distinct peaks at 1420 and 900 cm^{-1}, corresponding to asymmetric stretching and out-of-plane bending of CO_3^{2-} [88–89]. The optimized product closely matches all major SPB-1 bands, confirming the formation of the same structural motifs. Repeated measurements yielded consistent spectra, demonstrating method reproducibility (Fig. S3).

Deviations from optimized electrolysis conditions produced clear spectral changes. At unsuitable current densities (<0.675 or >0.925 A cm^{-2}) or elevated temperatures, SPB-typical bands were diminished or absent, indicating reduced formation or thermal decomposition. Mildly suboptimal current density (0.725 A cm^{-2}) generated spectra partially resembling SPB-1, consistent with incomplete conversion. Adequate post-electrolysis stirring was also required: insufficient mixing (≤10 min) led to weak SPB features, supporting the need for sufficient reaction time for B–O–O–H formation. At very low temperatures (<−2.9 °C) or after prolonged standing (>240 min), additional signals at 1420 and 900 cm^{-1} appeared (Fig. 5), which matched carbonate reference spectra and were confirmed by a carbonate–product mixture (Fig. 3).

Although quantitative IR approaches such as PLS regression have been described [90], the present study focuses on qualitative and semi-quantitative interpretation. In this context, relative spectral purity can be inferred from the close correspondence of SPB-typical absorption features and absent of carbonate-related absorptions with those of the commercial reference. While absolute absorbance intensities depend on sample preparation, the presence and positions of characteristic bands are determined by chemical structure. The very high spectral similarity observed between the electrochemically synthesized product and commercial SPB-1, together with an identical active oxygen content (≈14%), provides convergent evidence that the product obtained is of high purity.

3.3. *Mechanistic insight into the electrosynthesis of perborate*

Electrochemical behavior of carbonate-, bicarbonate-, and borate-containing electrolytes on BDD (CV analysis). To establish the electrochemical processes accessible on the BDD anode and to define the anodic potential window relevant for perborate formation, cyclic voltammetry (CV) was performed in electrolytes containing carbonate, bicarbonate, hydroxide, and borate species (Fig. 6 and Figs. S6–S7). Potentials are reported versus the reversible hydrogen electrode (RHE) to enable comparison across electrolytes of different pH.

The concentrations used for CV measurements were selected to reflect the chemical conditions applied during galvanostatic electrosynthesis. Na_2CO_3 (130 g L^{-1}) and $NaHCO_3$ (30 g L^{-1}) were employed as the primary electrolyte and co-species, respectively, consistent with their roles during perborate formation. For single-species measurements, carbonate or bicarbonate concentrations of 130 g L^{-1} were used to maintain a comparable chemical environment. A 1 M NaOH solution was included as an alkaline reference electrolyte to benchmark oxygen evolution behavior and to ensure sufficient ionic conductivity. Although the investigated electrolytes differ in absolute conductivity, the CV analysis focuses on anodic onset potentials and qualitative trends rather than direct comparison of current magnitudes.

Fig.6 shows that the anodic response on BDD depends strongly on electrolyte composition. The carbonate/bicarbonate mixture exhibits the earliest onset of anodic current, followed by carbonate and NaOH electrolytes, which display pronounced anodic current increase, characteristic of high-potential oxidation processes on BDD. In contrast, bicarbonate-only electrolyte shows a significantly suppressed anodic response, while borate-only electrolyte exhibits only minimal current over the investigated potential range. These results indicate that efficient anodic oxidation on BDD is strongly influenced by carbonate speciation, whereas borate does not undergo direct anodic oxidation at an appreciable rate under the applied conditions. Upon addition of borax into carbonate/bicarbonate solution, the anodic wave remains or shifts to higher potentials and the current is correspondingly suppressed (Fig. S6), indicating that borate species do not directly participate in the electrochemical oxidation step but instead interact with electrogenerated oxidants and/or modify the electrode–electrolyte interface, thereby increasing the effective overpotential.

Influence of electrolyte composition. To probe the role of carbonate species in the generation of reactive oxygen species (ROS) relevant for perborate formation, the carbonate-containing electrolyte was systematically replaced with NaOH (0.04–40 g L^{-1}, pH 11–14). In all cases, no solid precipitate was observed after electrolysis. Iodometric titration of aliquots withdrawn after one-third, two-thirds, and the full applied charge revealed no detectable active oxygen content. This indicates that either oxygen evolution dominates under these conditions or that only trace, short-lived peroxide species are formed, insufficient for productive conversion into stable perborate.

Consistent with these observations, cyclic voltammetry (Fig.6) reveals that NaOH exhibits a pronounced anodic current increase characteristic of the oxygen evolution reaction (OER; $4\ OH^- \rightarrow O_2 + 2\ H_2O + 4\ e^-$), owing to the increasing concentration of NaOH and OH− absorption [93]. Consequently, in electrolytes containing only NaOH and borate, perborate formation is not observed Table 1.

In contrast, electrolytes containing carbonate or bicarbonate consistently produced measurable ROS, as confirmed by iodometric titration (Table S7). However, an isolable solid corresponding to SPB-1 was obtained only in carbonate-rich media. When bicarbonate was used as the sole electrolyte, electrolysis yielded a solid exhibiting only a weak perborate fingerprint (Fig. S5) together with a very low active oxygen content (0.2%) and extremely low yield (0.2%). This indicates that bicarbonate alone does not support efficient perborate formation.

This behavior is consistent with previous studies on carbonate-mediated electrochemical oxidant generation. Fan et al. [100] reported that sodium bicarbonate solutions perform significantly worse than carbonate solutions for electrochemical water oxidation to hydrogen peroxide, an effect attributed to differences in solution chemistry and effective alkalinity. Similarly, Seiz et al. [63] identified a favorable pH window (≈11–13.5) for the formation of

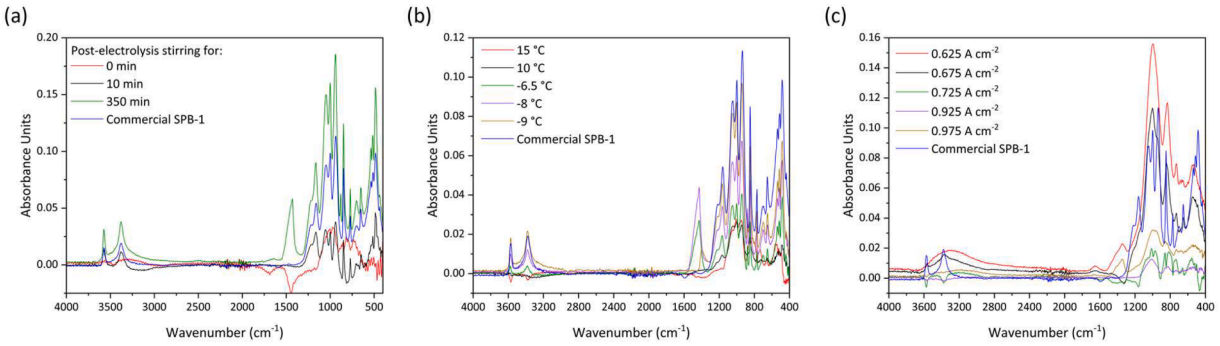

Fig. 5. FTIR spectra of perborate-related products generated under non-optimized conditions, including (a) improper post-electrolysis stirring time, (b) deviations in internal cell temperature and (c) improper current density.

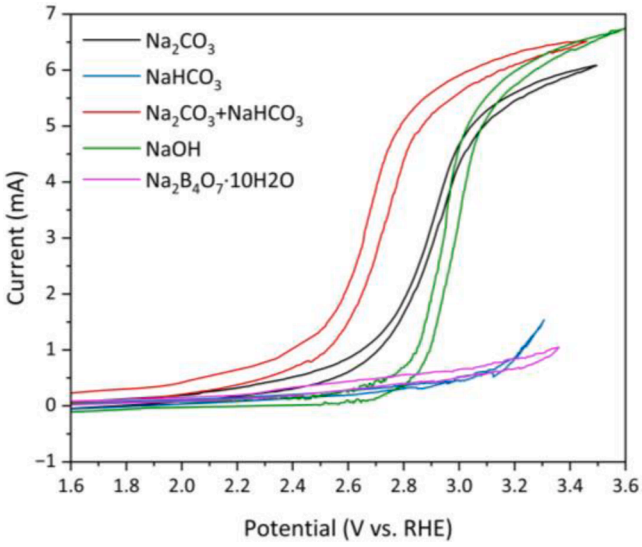

Fig. 6. Cyclic voltammograms recorded on a BDD anode in Na_2CO_3 (130 g L^{-1}), $NaHCO_3$ (130 g L^{-1}), Na_2CO_3 + $NaHCO_3$ (130 + 30 g L^{-1}), NaOH (1 M), and $Na_2B_4O_7{\cdot}10H_2O$ (40 g L^{-1}) electrolytes at 0.1 V s^{-1} and room temperature. Potentials are reported versus RHE.

Table 1
Electrolyte-dependent formation of sodium perborate: Influence of NaOH, Na_2CO_3, $NaHCO_3$, and K^+ salts on solid formation and SPB yield. Conducted at 0.875 A cm^{-2}, 8 *F*, 2 °C, and 550 rpm.

S2	Electrolyte Composition	*c* (g/L)	Solid Formation	Yield (%)
1	NaOH	0.04	No	0
2	NaOH	0.4	No	0
3	NaOH	4	No	0
4	NaOH	8	No	0
5	NaOH	20	No	0
6	NaOH	40	No	0
7	Na_2CO_3	130	Yes	13.5
8	K_2CO_3	130	No	0
9	$NaHCO_3$	130	Yes	0
10	$KHCO_3$	130	No	0
11	K_2CO_3+$KHCO_3$	130+30	No	0
12	K_2CO_3+$NaHCO_3$	130+30	No	0
13	Na_2CO_3+$KHCO_3$	130+30	Yes	16.1
14	Na_2CO_3+$NaHCO_3$	130+30	Yes	21.9

peroxodicarbonate ($C_2O_6^{2-}$), suggesting that sufficiently alkaline conditions are required to sustain carbonate-derived oxidant pathways. In this context, the suppressed anodic response observed for bicarbonate electrolytes in the CV measurements (Fig. S6) is consistent with limited oxidant generation under bicarbonate-buffered conditions, while the addition of borax partially restores anodic activity in bicarbonate solutions, likely through modification of local pH and interfacial equilibria rather than direct electrochemical participation of borate.

In mixed carbonate–bicarbonate systems, combining Na_2CO_3 (130 g L^{-1}) and $NaHCO_3$ (30 g L^{-1}) resulted in a higher SPB-1 yield than carbonate alone. Correspondingly, bicarbonate-containing electrolytes exhibit an earlier anodic current onset than carbonate-only systems. This synergistic behavior is consistent with literature reports describing bicarbonate as an accelerating co-species that enhances overall oxidant productivity when carbonate is present [19,92–94]. In such systems, bicarbonate likely functions as a buffering and proton-transfer mediator, facilitating indirect oxidation pathways without acting as the primary electroactive species.

Influence of the Cation (Na^+ vs. K^+). Replacing sodium salts with the corresponding potassium salts resulted in solutions with high active oxygen content (Table S7) but no solid precipitation. Cyclic voltammetry reveals that K^+-containing electrolytes generally display a positive shift in anodic onset potential relative to the all-sodium systems (Fig. S7), the presence of substantial anodic currents confirms that oxidant generation is not completely suppressed in potassium-based electrolytes.

This observation is consistent with previous studies reporting that potassium carbonate electrolytes can sustain high concentrations of dissolved hydrogen peroxide due to the higher solubility and weaker hydration shell of potassium salts compared to their sodium analogues [63,91, 95–96]. Accordingly, the absence of isolable perborate in K^+ systems cannot be attributed to insufficient electrochemical oxidant formation. Instead, it reflects limitations in the subsequent non-electrochemical steps required for perborate formation and isolation. Potassium perborate species are known to exhibit higher solubility and lower solid-state stability than sodium perborate [97], which disfavors effective trapping of H_2O_2 by borate and suppresses precipitation from solution. As a result, any transiently formed potassium perborate is expected to remain in solution and to undergo rapid back-conversion to borate and hydrogen peroxide, preventing accumulation of a stable solid product.

Effect of Carbonate Concentration and Peroxodicarbonate Supplementation. The yield of perborate strongly depended on the carbonate–bicarbonate ratio (Table 2). At low electrolyte strength, the reaction was severely limited: at 0.25 × concentration, no detectable SPB was formed, and even at 0.5 × the yield remained low at 12.4%, indicating insufficient carbonate to sustain productive ROS generation. Increasing the concentration to 0.75 × improved the yield to 15.4%, and the optimized 1 × formulation (130 + 30 g L^{-1}) provided the highest yield of 21.9%. Slightly higher carbonate loading (1.25 ×) led to only marginal improvement (22.4%), showing that the operational optimum is narrow. Further increases caused a decline in performance: yields dropped to 15.4% at 1.5 × and 13.0% at 1.75 ×, and no SPB formed at 2 ×, where bulk salt crystallization reduced electrolyte mobility and

Table 2
Effect of carbonate/bicarbonate concentration on SPB yield: systematic variation of electrolyte strength relative to the standard composition. Conducted at 0.875 A cm^{-2}, 8 *F*, 2 °C, and 550 rpm.

Entry	*c* (g/L)	Concentration Factor	Yield (%)
1	32.5+7.5	0.25	0
2	65+15	0.5	12.4
3	97.5+22.5	0.75	15.4
4	130+30	1	21.9
5	162.5+37.5	1.25	22.4
6	195+45	1.5	15.4
7	227.5+52.5	1.75	13.0
8	260+60	2	0

effectively inhibited electrolysis. Overall, both insufficient and excessive carbonate suppress SPB formation, and the optimized composition represents a practical balance between ROS generation capability and acceptable mass transport.

These observations correlate strongly with the anode potential trends. At low carbonate concentration (0.25 ×), the apparent anode potential was extremely high (~9.9 V vs RHE), indicating severe ohmic limitation and inefficient electrolysis. Increasing carbonate concentration to the optimized level reduced the required anode potential to ~5.9 V, consistent with improved conductivity and more efficient oxidant generation. At higher concentrations (>1 ×), the anode potential increased only modestly, suggesting that the decline in yield is not electrochemical in origin but instead arises from mass-transport limitations and phase behavior (increased viscosity and salt crystallization). Overall, the optimized electrolyte composition represents a balance between sufficient ionic conductivity and favorable transport conditions for peroxy-intermediate formation and stabilization.

Experiments using externally prepared peroxodicarbonate according to the method of Waldvogel and Gooßen (Peroxodicarbonate Preparation Electrolyte) further confirm this hypothesis [63]. For clarity, the standard Perborate Synthesis Electrolyte (PBE, 130 g L^{-1} Na_2CO_3 + 30 g L^{-1} $NaHCO_3$) and the Peroxodicarbonate Preparation Electrolyte (PDE, 95.4 g L^{-1} Na_2CO_3 + 155.5 g L^{-1} K_2CO_3 + 22.5 g L^{-1} $KHCO_3$) are referred to by these abbreviations throughout.

When PDE is directly mixed with PBE before electrolysis (Table 3, Entries 4–6), the SPB yield decreases markedly, consistent with the well-established inhibiting effect of excess K^+ on precipitation. In contrast, when PDE is first electrolyzed to generate fresh peroxodicarbonate and the resulting oxidant solution is added into PBE (Entries 1–3), the perborate yield increases. The strongest effect occurs at moderate addition (Entry 2), where the yield reaches 47.0%—surpassing the PBE-only control (Entry 10, 41.5%) even though the added solution originates from a K^+-containing medium. This demonstrates that supplemental, freshly generated peroxodicarbonate promotes perborate formation by supplying additional H_2O_2 and thereby increase the yield of SPB despite the presence of higher concentration of K^+.

Table 3
Influence of externally added peroxodicarbonate on sodium perborate yield. Entries 1–3 use freshly generated peroxodicarbonate (PDE electrolyzed before mixing with PBE), whereas Entries 4–6 use non-electrolyzed PDE. Entries 7–9 replace PBE with deionized water to test carbonate dependency. All experiments were performed at 0.875 A cm^{-2}, 8 *F*, 2 °C, and 550 rpm.

Entry	Electrolyte Composition	Yield (%)
1	28 mL 0.3125 M peroxodicarbonate + 78 mL PBE	30.7
2	46 mL 0.5275 M peroxodicarbonate + 54 mL PBE	47.0
3	80 mL 0.685 M peroxodicarbonate + 20 mL PBE	18.8
4	28 mL PDE + 78 mL PBE	22.2
5	46 mL PDE + 54 mL PBE	15.4
6	80 mL PDE + 20 mL PBE	0.7
7	28 mL 0.625 M peroxodicarbonate + 78 mL deionized water	0
8	68 mL 0.58 M peroxodicarbonate + 32 mL deionized water	0
9	85 mL 0.686 M peroxodicarbonate + 25 mL deionized water	0
10	100 mL PBE	41.5

Control experiments using water as the solvent (Entries 7–9) yield no solid product, confirming that carbonate is essential: it participates in peroxodicarbonate generation and also provides the high-ionic-strength environment necessary for SPB precipitation. Moreover, ex-cell peroxodicarbonate mixed with borax in the absence of electrolysis (Table S8) produces no precipitate, indicating that electrolysis is required to generate the reactive, short-lived oxidants in-situ that drive the conversion of borate to stable perborate.

Combined cyclic voltammetry and galvanostatic studies demonstrate that sodium perborate formation on BDD does not proceed via direct electrochemical oxidation of borate. Instead, the process follows an **indirect oxidation pathway**, in which electrogenerated oxidizing species are first formed at the anode and subsequently react with borate in solution. Accordingly, the overall mechanism can be divided into two sequential steps:

(i) an **electrochemical step**, involving the generation of peroxide-containing oxidants, and
(ii) a **non-electrochemical step**, in which hydrogen peroxide complexes with borate to form perborate.

The exact identity of the primary oxidizing intermediates generated at the BDD anode cannot be conclusively determined from the present study. However, prior mechanistic work by Fan *et al.* (Nature, 2022) [93] on carbonate-mediated electrochemical water oxidation provides strong evidence for the formation of carbonate-derived radical and peroxy-intermediates. In that work, the presence of carbonate radicals ($CO_3^{\bullet-}$) was confirmed by EPR spectroscopy, and peroxymonocarbonate (HCO_4^-) was identified by isotope-labeling experiments, supporting a pathway in which hydrogen peroxide is produced via carbonate-mediated electrochemical water oxidation.

However, the possible involvement of hydroxyl radicals (•OH) and peroxodicarbonate ($C_2O_6^{2-}$) has been reported in related electrochemical syntheses of hydrogen peroxide using BDD anodes in carbonate-containing electrolytes.

Based on these considerations, the proposed reaction pathway is summarized in Fig. 7 and Eqs. (1)–(10). Hydrogen peroxide can be generated electrochemically via hydrolysis of peroxodicarbonate or peroxymonocarbonate species formed from carbonate oxidation (Eqs.

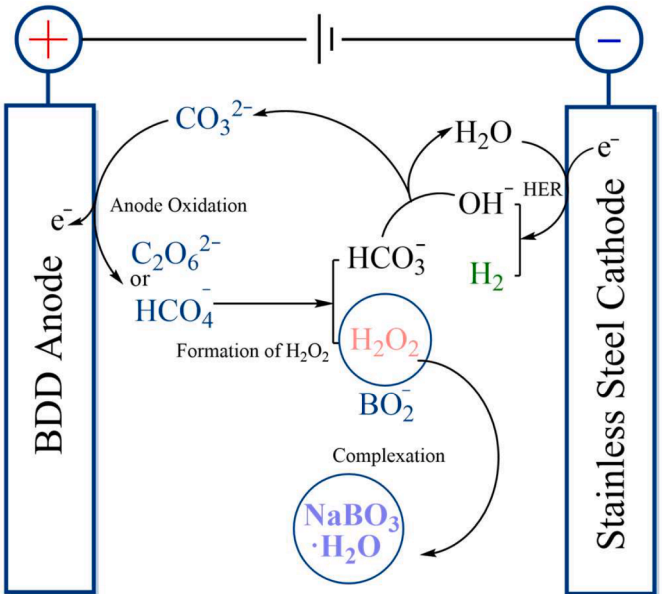

Fig. 7. Proposed electrochemical pathway for sodium perborate formation by peroxodicarbonate generation at BDD.

1–7). In the subsequent chemical step, hydrogen peroxide complexes with borate to form a tetrahedral perborate species (Eq. 8). The cathodic reaction corresponds to hydrogen evolution (Eq. 9), while bicarbonate formed during peroxide generation is reconverted to carbonate by reaction with hydroxide generated at the cathode, thereby closing the carbonate cycle (Eq. 10).

(1) Electrochemical formation of H_2O_2:
a) Via hydrolysis of peroxodicarbonate [12,27,60–61,98–101]:

$$2CO_3^{2-} \rightarrow C_2O_6^{2-} + 2e^- \quad (1)$$

$$\text{Or } H_2O \rightarrow \cdot OH + H^+ + e^- \quad (2)$$

$$2HCO_3^- + 2\cdot OH \rightarrow C_2O_6^{2-} + 2H_2O \quad (3)$$

$$C_2O_6^{2-} + 2H_2O \rightarrow 2HCO_3^- + H_2O_2 \quad (4)$$

b) Via hydrolysis of percarbonate [91,92]:

$$CO_3^{2-} \rightarrow CO\cdot_3^- + e^- \quad (5)$$

$$CO\cdot_3^- + H_2O \rightarrow HCO_4^- + H^+ + e^- \quad (6)$$

$$HCO_4^- + H_2O \rightarrow 2HCO_3^- + H_2O_2 \quad (7)$$

(2) Complexation of H_2O_2 with borate to form perborate [12,102]:

$$BO_2^- + H_2O_2 \rightarrow (BO_2^- \cdot H_2O_2) \quad (8)$$

(3) Hydrogen evolution reaction on cathode:

$$2H_2O + 2e^- \rightarrow H_2(g) + 2OH^- \quad (9)$$

(4) The bicarbonate anion generated during hydrolysis reacts with hydroxide ions formed at the cathode to regenerate carbonate, thereby completing a closed carbonate cycle:

$$HCO_3^- + OH^- \rightarrow CO_3^{2-} + H_2O \quad (10)$$

4. Conclusion

This work establishes a robust electrochemical route for the synthesis of sodium perborate monohydrate (SPB-1) from concentrated carbonate/bicarbonate electrolytes using a boron-doped diamond (BDD) anode. Through systematic variation of temperature, current density, applied charge, and post-electrolysis mixing, a narrow but reproducible operational window was identified that enables efficient perborate formation. Under optimized conditions (internal temperature 3.5 °C, current density 0.825–0.875 A cm^{-2}, the applied charge 24–26 *F*, vigorous stirring, and ≥20 min post-electrolysis coordination), the process delivers SPB-1 with an isolated yield of 80%, an active oxygen content of 14%, and a current efficiency of 26%, energy consumption of 2.46 kWh mol^{-1} or 24.6 kWh kg^{-1} with excellent run-to-run reproducibility.

Electrochemical analysis combining cyclic voltammetry and galvanostatic anode potential measurements provides mechanistic insight into this performance. The data demonstrate that carbonate oxidation on BDD occurs at highly positive potentials overlapping with the oxygen evolution region, explaining both the necessity of a sufficiently high anodic driving force and the intrinsic competition with OER. The optimal current density corresponds to a compromise in which carbonate-derived peroxy intermediates are generated efficiently without excessive diversion of current to oxygen evolution. Temperature-dependent potential measurements further indicate that low-temperature operation increases the apparent anode potential due to kinetic and transport effects, while simultaneously stabilizing peroxy intermediates and SPB-1, thereby enhancing net yield. These findings rationalize why BDD, with its wide anodic potential window and high stability, enables productive perborate synthesis whereas platinum anodes—operating at substantially lower potentials and favoring OER—do not.

Table 4
Comparison of electrochemical sodium perborate synthesis reported in the literature.

Study	Anode Material	SPB Concentration / Yield	Key limitations
Arndt et al. [18]	Pt	20–27 g L^{-1}	Limited yield, Pt stability, strong OER competition
Mollard et al. [20]	Pt	≤25 g L^{-1}	Low reproducibility, pretreatment of borax
González Pérez et al. [3]	Pt/BDD	83.9 mmol L^{-1} (no isolation)	No solid SPB isolated, concluded BDD unsuitable, complex process
This work	BDD	33.5 g L^{-1} (335.6 mmol L^{-1})	OER still limits current efficiency

In comparison with prior reports, the present protocol represents a substantial advance in both productivity and practicality. Early studies by Arndt and related work achieved only modest isolated perborate yields. More recently, González Pérez et al. [3] reported that BDD was ineffective for the oxidation of boron compounds and carbonate, yielding only trace perborate concentrations (0.2 mmol L^{-1}). In contrast, the present work demonstrates that, under appropriately tuned electrolyte composition and operating conditions, BDD enables efficient perborate formation and direct isolation of solid SPB-1. An isolated product concentration of 33.5 g L^{-1} was obtained, corresponding to 335.6 mmol L^{-1} on a molar basis, placing this study among the highest productivities reported to date for electrochemical sodium perborate synthesis (Table 4).

From a sustainability perspective, the method eliminates the need for externally produced hydrogen peroxide, instead generating the oxidizing equivalent electrochemically from carbonate, an inexpensive and widely available feedstock. Direct precipitation of SPB-1 from the reaction medium further simplifies downstream processing. While the current efficiency is inherently limited by competition with OER, it is already reasonable for a high-potential anodic process. Future improvements may be achieved through electrolyte engineering (e.g., targeted additives to suppress OER), surface modification of BDD to tune interfacial reactivity, and reactor designs that minimize ohmic losses and enhance mass transport—strategies that are well aligned with scale-up considerations.

Overall, this study provides a mechanistically grounded and experimentally validated framework for SPB-1 electrosynthesis. By integrating electrochemical diagnostics with systematic process optimization, it establishes BDD-based electrolysis as a promising platform for sustainable oxidant production and offers a clear pathway toward further efficiency improvements and industrial implementation.

Data availability

Primary data will be made available on request.

CRediT authorship contribution statement

Ziqi Teng: Writing – review & editing, Writing – original draft, Visualization, Validation, Methodology, Investigation, Data curation. **Finn Moeller:** Writing – review & editing, Writing – original draft, Validation, Project administration, Methodology. **Siegfried R.**

Waldvogel: Writing – review & editing, Writing – original draft, Supervision, Funding acquisition, Conceptualization.

Declaration of competing interest

The authors declare the following financial interests/personal relationships which may be considered as potential competing interests:

Siegfried R. Waldvogel reports financial support was provided by Deutsche Forschungsgemeinschaft. If there are other authors, they declare that they have no known competing financial interests or personal relationships that could have appeared to influence the work reported in this paper.

Acknowledgement

Funded by the Deutsche Forschungsgemeinschaft (DFG, German Research Foundation) under Germany's Excellence Strategy – EXC-2033-390677874 – RESOLV, and Wa1276/23-2 – UNODE.

Supplementary materials

Supplementary material associated with this article can be found, in the online version, at doi:10.1016/j.electacta.2026.148424.

References

[1] A. Mckillop, W.R. Sanderson, Sodium perborate and sodium percarbonate: cheap, safe and versatile oxidising agents for organic synthesis, Tetrahedron 51 (1995) 6145–6166, https://doi.org/10.1016/0040-4020(95)00304-Q.
[2] G.W. Kabalka, T.M. Shoup, N.M. Goudgaon, Sodium perborate: a mild and convenient reagent for efficiently oxidizing organoboranes, J. Org. Chem. 54 (1989) 5930–5933, https://doi.org/10.1021/jo00286a026.
[3] O. González Pérez, F.B. Martínez, J. Bisang, Assessment of the electrochemical production of sodium perborate, J. Chem. Technol. Biotechnol. 100 (2025) 1693–1701, https://doi.org/10.1002/jctb.7899.
[4] Y.M. Indi, A. Wasif, Sodium perborate bleaching of cotton by using tetraacetyl ethylenediamine activator, Indian J. Fibre Text. Res. 43 (2018) 120–125. https://www.researchgate.net/publication/324159421.
[5] S.S. Block, Disinfection, Sterilization, and Preservation, Lippincott Williams & Wilkins: Philadelphia, 2001 fifth ed.
[6] L.V. Macey-Dare, B. Williams, Bleaching of a discoloured non-vital tooth: use of a sodium perborate/water paste as the bleaching agent, Int. J. Paed Dent. 7 (1997) 35–38, https://doi.org/10.1111/j.1365-263X.1997.tb00271.x.
[7] Belinka Perkemija, Sodium perborate. https://www.belinka-perkemija.com/en/, 2016.
[8] A. Mckillop, W.R. Sanderson, Sodium perborate and sodium percarbonate: further applications in organic synthesis, J. Chem. Soc. Perkin Trans. 1 (2000) 471–476, https://doi.org/10.1039/A804579H.
[9] J.F. Bower, C.J. Martin, D.J. Rawson, A.M.Z. Slawin, J.M.J. Willianms, Diastereoselective conversion of sulfides into sulfoxides. 1,5- and 1,6-asymmetric induction, J. Chem. Soc. Perkin Trans. 1 (1995) 333–342, https://doi.org/10.1039/P19960000333.
[10] M. Begtrup, P. Vedsø, Preparation of N-hydroxyazoles by oxidation of azoles, J. Chem. Soc. Perkin Trans. 1 (1995) 243–247, https://doi.org/10.1039/P19950000243.
[11] B.P. Bandgar, S.I. Shaikh, S. Iyer, Oxidative deoximation with sodium perborate, Synth. Commun. 26 (6) (1996) 1163–1168, https://doi.org/10.1080/00397919608003724.
[12] A. Regner, Electrochemical Processes in Chemical Industries, Artia; Constable and Co. Ltd., Prague, 1957.
[13] Umwelt Bundesarmt, German notes on BAT of the production of large volume solid inorganic chemicals: sodium perborate. https://www.umweltbundesamt.de/publikationen, 2001.
[14] H.R. Carveth, Preparation of sodium perborate, US1716874A (1929).
[15] K.H. Büchel, H-H. Moretto, P. Woditsch, Industrial Inorganic Chemistry, Wiley-VCH: Weinheim, 2000 second ed.
[16] D.F. Altimier, N. Falls, W. Klabunde, Production of sodium perborate, US2828183A (1958).
[17] a) S.R. Waldvogel, B. Janza, Renaissance of electrosynthetic methods for the construction of complex molecules, Angew. Chem. Int. Ed 53 (2014) 7122–7123, https://doi.org/10.1002/anie.201405082;
b) M.D. Kärkäs, Electrochemical strategies for C–H functionalization and C–N bond formation, Chem. Soc. Rev. 47 (2018) 5786–5865, https://doi.org/10.1039/C7CS00619E;
c) C. Zhu, N.W.J. Ang, T.H. Meyer, Y. Qiu, L. Ackermann, Organic electrochemistry: molecular syntheses with potential, ACS Cent. Sci. 7 (2021) 415–431, https://doi.org/10.1021/acscentsci.0c01532;
d) M.C. Leech, K. Lam, A practical guide to electrosynthesis, Nat. Rev. Chem. 6 (2022) 275–286, https://doi.org/10.1038/s41570-022-00372-y;
e) A. Wiebe, T. Gieshoff, S. Möhle, E. Rodrigo, M. Zirbes, S.R. Waldvogel, Electrifying organic synthesis, Angew. Chem. Int. Ed 57 (2018) 5594–5619, https://doi.org/10.1002/anie.201711060;
f) S.B. Beil, D. Pollok, S.R. Waldvogel, Reproducibility in electroorganic synthesis—Myths and misunderstandings, Angew. Chem. Int. Ed 60 (2021) 14750–14759, https://doi.org/10.1002/anie.202014544;
g) S. Möhle, M. Zirbes, E. Rodrigo, T. Gieshoff, A. Wiebe, S.R. Waldvogel, Modern electrochemical aspects for the synthesis of value-added organic products, Angew. Chem. Int. Ed 57 (2018) 6018–6041, https://doi.org/10.1002/anie.201712732;
h) B.K. Peters, K.X. Rodriguez, S.H. Reisberg, S.B. Beil, D.P. Hickey, Y. Kawamata, M. Collins, J. Starr, L. Chen, S. Udyavara, K. Klunder, T.J. Gorey, S. L. Anderson, M. Neurock, S.D. Minteer, P.S. Baran, Scalable and safe synthetic organic electroreduction inspired by Li-ion battery chemistry, Science 363 (2019) 838–845, https://doi.org/10.1126/science.aav5606;
i) D. Pollok, S.R. Waldvogel, Electro-organic synthesis – a 21st century technique, Chem. Sci. 11 (2020) 12375–12592, https://doi.org/10.1039/D0SC01848A.
[18] K. Arndt, Elektrolytische gewinnung von Perborat, Z. Elektrochem 22 (1916) 63–64, https://doi.org/10.1002/bbpc.19160220303.
[19] O. Liebknecht, Electrolytic process of making Alkali perborate, US1235905A (1917).
[20] P. Mollard, Process of making sodium perborate by electrolysis, US3038842A (1962).
[21] N.S. Raghavendran, K.C. Narasimham, Electrolytic preparation of sodium perborate, Bull. Electrochem. 4 (1988). https://cecri.csircentral.net/1500/1/55-1988.pdf.
[22] M.Mohan Rao, N.S. Raghavendran, K.C. Narasimham, Preparation of sodium perborate by electrochemical methode, Trans. SAEST 35 (2000). https://cecri.csircentral.net/1044/1/120-2000.pdf.
[23] H. Mistry, A.S. Varela, S. Kühl, P. Strasser, B.R. Cuenya, Nanostructured electrocatalysts with tunable activity and selectivity, Nat. Rev. Mater 1 (2016) 16009, https://doi.org/10.1038/natrevmats.2016.9.
[24] S. Bawari, N.T. Narayanan, J. Mondal, Insights into the reaction pathways of platinum dissolution and oxidation during electrochemical processes, Electrochem. commun. 147 (2023) 107440, https://doi.org/10.1016/j.elecom.2023.107440.
[25] J. Lee, J.H. Bang, Reliable counter electrodes for the hydrogen evolution reaction in acidic media, ACS. Energy Lett. 5 (2020) 2706–2710, https://doi.org/10.1021/acsenergylett.0c01537.
[26] D.J. Myers, X. Wang, M.C. Smith, K.L. More, Potentiostatic and potential cycling dissolution of polycrystalline platinum and platinum nano-particle fuel cell catalysts, J. Electrochem. Soc 165 (2018) F3178–F3190, https://doi.org/10.1149/2.0211806jes.
[27] D.C. Johnson, D.T. Napp, S. Bruckenstein, A ring-disk electrode study of the current/potential behaviour of platinum in 1.0 M sulphuric and 0.1 M perchloric acids, Electrochim. Acta 15 (1970) 1493–1509, https://doi.org/10.1016/0013-4686(70)80070-6.
[28] D. A. J. Rand and R. Woods, Journal of electroanalytical chemistry and interfacial electrochemistry 35 (1972), 209-218, https://doi.org/10.1016/S0022-0728(72)80308-5.
[29] K. Kinoshita, J.T. Lundquist, P. Stonehart, Potential cycling effects on platinum electrocatalyst surfaces, J. Electroanal. Chem. Interfacial. Electrochem. 48 (1973) 157–166, https://doi.org/10.1016/S0022-0728(73)80257-8.
[30] X.P. Wang, R. Kumar, D.J. Myers, Effect of voltage on platinum dissolution: relevance to polymer electrolyte fuel cells, Electrochem. Solid-State Lett. 9 (2006) A225–A227, https://doi.org/10.1149/1.2180536.
[31] G. Kokkinidis, N. Xonoglou, Comparative study of the electrocatalytic influence of underpotential heavy metal adatoms on the anodic oxidation of monosaccharides on Pt in acid solutions, Bioelectrochem. Bioenerg. 14 (1985) 375–387, https://doi.org/10.1016/0302-4598(85)80010-6.
[32] U.S. Geological Survey. Mineral Commodity Summaries, Platinum-Group Metals, 2025.
[33] S. Cherevko, N. Kulyk, K.J.J. Mayrhofer, Durability of platinum-based fuel cell electrocatalysts: dissolution of bulk and nanoscale platinum, Nano Energy 29 (2016) 275–298, https://doi.org/10.1016/j.nanoen.2016.03.005.
[34] V.S. Vavilov, P.N. Lebedev, Diamond as a material in solid State electronics, MRS Online Proc. Libr. 242 (1992) 87–95, https://doi.org/10.1557/PROC-242-87.
[35] Yu.V. Pelskov, A.Ya. Sakharova, M.D. Krotova, L.L. Bouilov, B.V. Spitsyn, Photoelectrochemical properties of semiconductor diamond, J. Electroanal. Chem. 228 (1987) 19–27, https://doi.org/10.1016/0022-0728(87)80093-1.
[36] Yu.Y. Pelskov, Synthetic diamond in electrochemistry, Russ. Chem. Rev. 68 (1999) 381–392, https://doi.org/10.1070/RC1999v068n05ABEH000494.
[37] Yu.Y. Pelskov, Electrochemistry of diamond: a review, Russ. Chem. Rev. 38 (2002) 1275–1291, https://doi.org/10.1023/A:1021651920042.
[38] M. Panizza, G. Cerisola, Application of diamond electrodes to electrochemical processes, Elctrochim. Acta 51 (2005) 191–199, https://doi.org/10.1016/j.electacta.2005.04.023.
[39] G.M. Swain, A.B. Anderson, J.C. Angus, Diamond electrodes: diversity and maturity, MRS Bull. 39 (06) (2014) 525–535, https://doi.org/10.1557/mrs.2014.94.
[40] H.B. Martin, A. Argoitia, U. Landau, A.B. Anderson, J.C. Angus, Hydrogen and oxygen evolution on Boron-doped diamond electrodes, J. Electrochem. Soc. 143 (1996) L133–L136. https://iopscience.iop.org/article/10.1149/1.1836901.

[41] S.R. Waldvogel, S. Mentizi, A. Kirste, Boron-doped diamond electrodes for electroorganic chemistry, Top. Curr. Chem. 320 (2012) 1–31, https://doi.org/10.1007/128_2011_125.
[42] R. Ramesham, M.F. Rose, Electrochemical characterization of doped and undoped CVD diamond deposited by microwave plasma, Diam. Rebated Mater. 6 (1997) 17–27, https://doi.org/10.1016/S0925-9635(96)00593-6.
[43] S. Lips, S.R. Waldvogel, Use of boron-doped diamond electrodes in electro-organic synthesis, ChemElectroChem 6 (2019) 1649–1660, https://doi.org/10.1002/celc.201801620.
[44] N. Yang, S. Yu, J.V. Macpherson, Y. Einaga, H. Zhao, G. Zhao, G.M. Swain, X. Jiang, Conductive diamond: synthesis, properties, and electrochemical applications, Chem. Soc. Rev. 48 (2019) 157–204, https://doi.org/10.1039/C7CS00757D.
[45] G.M. Swain, R. Ramesham, The electrochemical activity of boron-doped polycrystalline diamond thin film electrodes, Anal. Chem. 65 (1993) 345–351. https://pubs.acs.org/doi/10.1021/ac00052a007.
[46] G.M. Swain, The use of CVD diamond thin films in electrochemical systems, Adv. Mater. 5 (1994) 388–392, https://doi.org/10.1002/adma.19940060511.
[47] B. Marselli, J. Garcia-Gomez, P.-A. Michaud, M.A. Rodrigo, C. Comninellis, Electrogeneration of hydroxyl radicals on boron-doped diamond electrodes, J. Electrochem. Soc. 150 (2003) D79–D83. https://iopscience.iop.org/article/10.1149/1.1553790/meta.
[48] C. Comninellis, Electrocatalysis in the electrochemical conversion/combustion of organic pollutants for waste water treatment, Electrochim. Acta 39 (1994) 1857–1862, https://doi.org/10.1016/0013-4686(94)85175-1.
[49] S.R. Waldvogel, B. Elsler, Electrochemical synthesis on boron-doped diamond, Electrochim. Acta 82 (2012) 434–443, https://doi.org/10.1016/j.electacta.2012.03.173.
[50] C. Heim, M. Ureña de Vivanco, M. Rajab, E. Müller, T. Letzel, B. Helmreich, Rapid inactivation of waterborne bacteria using boron-doped diamond electrodes, Int. J. Env.. Sci. Technol. 12 (2015) 3061–3070, https://doi.org/10.1007/s13762-014-0722-9.
[51] S. Fierro, Y. Honda, Y. Einaga, Influence of supporting electrolyte on the electrochemical oxidation of formic acid on boron-doped diamond electrodes, Bull. Chem. Soc. Jpn 86 (2013) 749–754, https://doi.org/10.1246/bcsj.20130008.
[52] D. Zollinger, U. Griesbach, H. Pütter, C. Comninellis, Electrochemical cleavage of 1,2-diphenylethanes at boron-doped diamond electrodes, Electrochem. Commun. 6 (2004) 605–608, https://doi.org/10.1016/j.elecom.2004.04.014.
[53] K.R. Saravanan, V. Selvamani, K. Kulangiappar, D. Velayutham, V. Suryanarayanan, Regioselective anodic α-methoxylation of 2-oxazolidinone on boron doped diamond in acidic methanol medium, Electrochem. Commun. 28 (2013) 31–33, https://doi.org/10.1016/j.elecom.2012.12.002.
[54] I.M. Malkowsky, U. Griesbach, H. Pütter, S.R. Waldvogel, Unexpected highly chemoselective anodic ortho-coupling reaction of 2,4-dimethylphenol on boron-doped diamond electrodes, Eur. J. Org. Chem. (2006) 4569–4572, https://doi.org/10.1002/ejoc.200600466.
[55] a) N. Schupp, T. Rücker, E. Glöckler, B. Wittgens, S.R. Waldvogel, Enhanced oxidative degradation of kraft lignin by highly concentrated peroxodicarbonate, ChemSusChem (2025) e202500741, https://doi.org/10.1002/cssc.202500741.b) S.R. Waldvogel, M. Zirbes, R. Neuber, T. Matthée, Process for the oxidation of carbon-containing organic compounds with electrochemically generated oxidizing agents and arrangement for carrying out the process, DE102018128228A1 (2020).
[56] A. Ziogas, J. Belda, H-J. Kost, J. Magomajew, R.A. Sperling, P. Wernig, Peroxodicarbonate: electrosynthesis and first directions to green industrial applications, Curr. Res. Green Sustain. Chem. 5 (2022), https://doi.org/10.1016/j.crgsc.2022.100341, 2666-0865.
[57] I. Kisacik, A. Stefanova, S. Ernst, H. Baltruschat, Oxidation of carbon monoxide, hydrogen peroxide and water at a boron doped diamond electrode: the competition for hydroxyl radicals, Phys. Chem. Chem. Phys. 15 (2013) 4616–4624, https://doi.org/10.1039/C3CP44643C.
[58] P.J. Espinoza-Montero, P. Alulema-Pullupaxi, B.A. Frontana-Uribe, C.E. Barrera-Diaz, Electrochemical production of hydrogen peroxide on Boron-doped diamond (BDD) electrode, Curr. Opin. Solid State Mater. Sci. 26 (2022) 100988, https://doi.org/10.1016/j.cossms.2022.100988.
[59] Irkham, A. Fiorani, G. Valenti, N. Kamoshida, F. Paolucci, Y. Einaga, Electrogenerated chemiluminescence by in situ production of coreactant hydrogen peroxide in carbonate aqueous solution at a boron-doped diamond electrode, J. Am. Chem. Soc. 142 (2020) 1518–1525, https://doi.org/10.1021/jacs.9b11842.
[60] M.S. Saha, T. Furuta, Y. Nishiki, Electrochemical synthesis of sodium peroxycarbonate at boron-doped diamond electrodes, Electrochem. Solid-State Lett. 6 (2003) D5–D7. https://iopscience.iop.org/article/10.1149/1.1576050.
[61] M.S. Saha, T. Furuta, Y. Nishiki, Conversion of carbon dioxide to peroxycarbonate at boron-doped diamond electrode, Electrochem. Commun. 6 (2004) 201–204, https://doi.org/10.1016/j.elecom.2003.11.014.
[62] E.J. Ruiz-Ruiz, Y. Meas, R. Ortega-Borges, J.L. Jurado Baizabal, Electrochemical production of peroxocarbonate at room temperature using conductive diamond anodes, Surf. Eng. Appl. Electrochem. 50 (2014) 478–484, https://doi.org/10.3103/S106837551406009X.
[63] A-K. Seitz, P.J. Kohlpaintner, T. van Lingen, M. Dyga, F. Sprang, M. Zirbes, S. R. Waldvogel, L.J. Gooßen, Concentrated aqueous peroxodicarbonate: efficient electrosynthesis and use as oxidizer in epoxidations, S-, and N-oxidations, Angew. Chem. Int. Ed 61 (2022), https://doi.org/10.1002/anie.202117563 e202117563.
[64] T. Rücker, N. Schupp, F. Sprang, T. Horsten, B. Wittgens, S.R. Waldvogel, Peroxodicarbonate – a renaissance of an electrochemically generated green oxidizer, Chem. Commun. 60 (2024) 7136–7147, https://doi.org/10.1039/D4CC02501F.
[65] A.-K. Seitz, T. van Lingen, M. Dyga, P.J. Kohlpaintner, S.R. Waldvogel, L. J. Gooßen, Amine oxidation by electrochemically generated peroxodicarbonate, Synlett 33 (2022) 1527–1531, https://doi.org/10.1055/a-1860-3405.
[66] F. Sprang, N. Schupp, P.J. Kohlpaintner, L.J. Gooßen, S.R. Waldvogel, E-Dakin reaction: oxidation of hydroxybenzaldehydes to phenols with electrochemically generated peroxodicarbonate, Green. Chem. 26 (2024) 5862–5868, https://doi.org/10.1039/D3GC04597H.
[67] P.J. Kohlpaintner, L. Marquart, L.J. Gooßen, S.R. Waldvogel, The oxidation of organo-boron compounds using electrochemically generated peroxodicarbonate, Eur. J. Org. Chem. 26 (2023), https://doi.org/10.1002/ejoc.202300220 e202300220.
[68] M. Zirbes, T. Graßl, R. Neuber, S.R. Waldvogel, Peroxodicarbonate as a green oxidizer for the selective degradation of kraft lignin into vanillin, Angew. Chem. Int. Ed 62 (2023), https://doi.org/10.1002/anie.202219217 e202219217.
[69] T. Horsten, S.R. Waldvogel, Halogen-free bleaching of shellac using electrochemically generated peroxodicarbonate, RSC Sustain. 2 (2024) 1963–1968, https://doi.org/10.1039/D4SU00228H.
[70] T. Rücker, T. Pettersen, H. Graute, B. Wittgens, T. Graßl, S.R. Waldvogel, Pilot scale electrolysis of peroxodicarbonate as an oxidizer for lignin valorization, ACS Sustain. Chem. Eng. 12 (2024) 11283–112910, https://doi.org/10.1021/acssuschemeng.4c02898.
[71] J. Li, H. Duan, Recent progress in energy-saving hydrogen production by coupling with value-added anodic reactions, Chem 10 (2024) 3008–3039, https://doi.org/10.1016/j.chempr.2024.08.009.
[72] E.A. Moges, C-Y. Chang, M-C. Tsai, W-N. Su, B.J. Hwang, Electrocatalysts for value-added electrolysis coupled with hydrogen evolution, EES Catal. 1 (2023) 413–433, https://doi.org/10.1039/d3ey00017f.
[73] G. Chen, X. Li, X. Feng, Upgrading organic compounds through the coupling of electrooxidation with hydrogen evolution, 61 (2022), e202209014, https://doi.org/10.1002/anie.202209014.
[74] B. Garlyyev, S. Xue, J. Fichtner, A.S. Bandarenka, C. Andronescu, Prospects of value-added chemicals and hydrogen via electrolysis, ChemSusChem 13 (2020) 2513–2521, https://doi.org/10.1002/cssc.202000339.
[75] G. Li, G. Han, L. Wang, et al., Dual hydrogen production from electrocatalytic water reduction coupled with formaldehyde oxidation via a copper-silver electrocatalyst, Nat. Commun. 14 (2023), https://doi.org/10.1038/s41467-023-36142-7.
[76] P. Phogat, B. Chand, Shreya, Hydrogen economy: pathways, production methods, and applications for a sustainable energy future, Sustain. Mater. Technol. 45 (2025) e01550, https://doi.org/10.1016/j.susmat.2025.e01550.
[77] D. Pollok, B. Gleede, A. Stenglein, S.R. Waldvogel, Preparative batch-type electrosynthesis: a tutorial, Aldrichimica Acta 54 (2021) 3–15, aldrichimica-acta-54-1.
[78] C.P. Chardon, T. Matthée, R. Neuber, M. Fryda, C. Comninellis, Efficient electrochemical production of peroxodicarbonate applying DIACHEM® diamond electrodes, ChemistrySelect. 2 (2017) 1037–1040, https://doi.org/10.1002/slct.201601583.
[79] B. Bertsch-Frank, K. Mueller, T. Lieser, High active oxygen content granulated sodium perborate product and method of making the same, US5094827A (1917).
[80] R.E. Mesmer, C.F. Baes Jr., F.H. Sweeton, Acidity measurements at elevated temperatures VI. Boric acid equilibriums, Inorg. Chem. 11 (1972) 537–543, https://doi.org/10.1021/ic50109a023.
[81] D.A. Palmer, P. Bénézeth, D.J. Wesolowski, Boric acid hydrolysis: a new look at the available data, Powerpl. Chem. 2 (2000) 261–264. https://www.osti.gov/etdeweb/biblio/20070326.
[82] A. Graff, E. Barrez1, P. Baranek1, M. Bachet, P. Bénézeth, Complexation of nickel ions by boric acid or (poly)borates, J. Solut. Chem. 46 (2017) 25–43, https://doi.org/10.1007/s10953-016-0555-x.
[83] Z. Pizer, C. Tihal, Peroxoborates, Interaction of boric acid and hydrogen peroxide in aqueous solution, Inorg. Chem. 26 (1987) 3639–3642, https://doi.org/10.1021/ic00268a046.
[84] I.V. Myachin, L.O. Kononov, Mixer design and flow rate as critical variables in flow chemistry affecting the outcome of a chemical reaction: a review, Inventions 8 (2023), https://doi.org/10.3390/inventions8050128.
[85] K. Iizuka, T. Kumeda, K. Suzuki, et al., Tailoring the active site for the oxygen evolution reaction on a Pt electrode, Commun. Chem. 5 (2022) 126, https://doi.org/10.1038/s42004-022-00748-7.
[86] S. Arya Devi, D. Philip, G. Aruldhas, Infrared, polarized Raman, and SERS spectra of borax, J. Solid. State Chem. 113 (1994) 157–162, https://doi.org/10.1006/jssc.1994.1354.
[87] J. Flanagan, W.P. Griffith, R.D. Powell, A.P. West, Vibrational spectra of alkali metal peroxoborates, Spectrochim. Acta A: Mol. Spectrosc. 45 (1989) 951–955, https://doi.org/10.1016/0584-8539(89)80153-9.
[88] J. Moros, R.J. Cassella, M.C. Barciela-Alonso, A. Moreda-Piñeiro, P. Herbello-Hermelo, P. Bermejo-Barrera, S. Garrigues, M. de la Guardia, Estuarine sediment quality assessment by fourier-transform infrared spectroscopy, Vib.Spectrosc 53 (2010) 204–213, https://doi.org/10.1016/j.vibspec.2010.03.001.
[89] S. Veerasingam, R. Venkatachalapathy, Estimation of carbonate concentration and characterization of marine sediments by Fourier Transform Infrared spectroscopy, Infrared Phys. Technol. 66 (2014) 136–140, https://doi.org/10.1016/j.infrared.2014.06.005.

[90] M. Khanmohammadi, N. Mashkuri, M. Rostami, A. Bagheri Garmarudi, Quantitative determination of sodium perborate and sodium percarbonate in detergent powders by infrared spectrometry, J. Anal. Chem. 67 (2012), https://doi.org/10.1134/S1061934812040089.
[91] L. Fan, X. Bai, C. Xia, et al., CO2/carbonate-mediated electrochemical water oxidation to hydrogen peroxide, Nat. Commun. 13 (2022) 2668, https://doi.org/10.1038/s41467-022-30251-5.
[92] D.E. Richardson, H. Yao, K.M. Frank, D.A. Bennett, Equilibria, kinetics, and mechanism in the bicarbonate activation of hydrogen peroxide: oxidation of sulfides by peroxymonocarbonate, J. Am. Chem. Soc. 122 (2000) 1729–1739, https://doi.org/10.1021/ja9927467.
[93] X. Yang, Y. Duan, J. Wang, H. Wang, H. Liu, D.L. Sedlak, Impact of peroxymonocarbonate on the transformation of organic contaminants during hydrogen peroxide in Situ chemical oxidation, Env.. Sci. Technol. Lett. 6 (2019) 781–786, https://doi.org/10.1021/acs.estlett.9b00682.
[94] C. Xia, S. Back, S. Ringe, Confined local oxygen gas promotes electrochemical water oxidation to hydrogen peroxide, Nat. Catal. 3 (2020) 125–134, https://doi.org/10.1038/s41929-019-0402-8.
[95] J.O'M. Bockris, A.K.N. Reddy, Modern Electrochemistry 2A: Fundamentals of Electrodics, Kluwe Academic/Plenum Publisher, New York, 2000.
[96] Y.Einaga Irkham, Oxidation of hydroxide ions in weak basic solutions using boron-doped diamond electrodes: effect of the buffer capacity, Analyst 144 (2019) 4499–4504, https://doi.org/10.1039/C9AN00505F.
[97] P.C. Alsgaard, Electrolytic production of sodium perborate, J. Phys. Chem. 26 (1922) 137–155, https://doi.org/10.1021/j150218a002.
[98] Z.-J. Pan, Y.-Y. Peng, Electrosynthesis of sodium perborate using air cathode, CIESC J. 47 (1996) 712–717. https://hgxb.cip.com.cn/CN/.
[99] O. González Pérez, J.M. Bisang, Peroxocarbonate production by using a divided cylindrical electrochemical reactor, Chem. Eng. Process 191 (2023) 109468, https://doi.org/10.1016/j.cep.2023.109468.
[100] T. Rücker, N. Schupp, F. Sprang, T. Horsten, B. Wittgens, S.R. Waldvogel, Peroxodicarbonate – a renaissance of an electrochemically generated green oxidizer, Chem. Commun. 60 (2024) 7136–7147, https://doi.org/10.1039/D4CC02501F.
[101] E.J. Ruiz, R. Ortega-Borges, J.L. Jurado, T.W. Chapman, Y. Meas, Simultaneous anodic and cathodic production of sodium percarbonate in aqueous solution, Electrochem. Solid St 12 (2009) E1–E4. https://iopscience.iop.org/article/10.1149/1.3005555.
[102] D.M. Kern, A polarographic study of the perborate complex, J. Am. Chem. Soc. 77 (1955) 5458–5462, https://doi.org/10.1021/ja01626a002.